International Journal of Heat and Mass Transfer 55 (2012) 7838–7846

Contents lists available at SciVerse ScienceDirect

International Journal of Heat and Mass Transfer

journal homepage: www.elsevier.com/locate/ijhmt

Optimization of peripheral finned-tube evaporators using entropy generation minimization

Bruno F. Pussoli [a], Jader R. Barbosa Jr. [a,*], Luciana W. da Silva [b], Massoud Kaviany [c]

[a] Polo – Research Laboratories for Emerging Technologies in Cooling and Thermophysics, Department of Mechanical Engineering, Federal University of Santa Catarina, Florianópolis, SC 88040-900, Brazil
[b] Embraco Compressors, Joinville, SC 89219-901, Brazil
[c] Department of Mechanical Engineering, University of Michigan, Ann Arbor, MI 48109-2125, USA

ARTICLE INFO

Article history:
Received 1 May 2012
Received in revised form 28 July 2012
Accepted 7 August 2012
Available online 16 September 2012

Keywords:
Heat exchanger
Porous media
Entropy generation
Optimization

ABSTRACT

The peripheral finned-tube (PFT) is a new geometry for enhanced air-side heat transfer under moisture condensate blockage (evaporators). It consists of individual hexagonal (peripheral) fin arrangements with radial fins whose bases are attached to the tubes and tips are interconnected with the peripheral fins. In this paper, experimentally validated semi-empirical models for the air-side heat transfer and pressure drop are combined with the entropy generation minimization theory to determine the optimal characteristics of PFT heat exchangers. The analysis is based on three independent parameters, i.e., porosity, equivalent particle diameter and particle-based Reynolds number. The total heat transfer rate is a fixed constraint. The optimal heat exchanger configurations, i.e., those in which the entropy generation number reaches a minimum, are calculated for constant heat flux and constant tube wall temperature boundary conditions. Performance evaluation criteria of fixed geometry, fixed face area and variable geometry were implemented. In all cases, it was possible to determine a combination of independent parameters that provided a minimum entropy generation rate.

1. Introduction

Finned-tube heat exchangers are widely employed as evaporators in direct-expansion vapor compression refrigeration systems. With the aim of increasing the air-side thermal conductance to meet space (volume) restrictions and pumping power constraints, a number of extended surface types have been proposed and reviewed in the literature [1,2]. Compilations of heat transfer and friction coefficient correlations for finned-tube geometries can be found in [3–5].

Wu et al. [6] proposed an extended surface geometry for enhanced performance under dehumidifying conditions. The peripheral finned-tube (PFT) geometry shown in Fig. 1 is a crossflow configuration in which the air-side is composed by hexagonal arrangements of open-pore cells formed by six radial fins whose bases are attached to the tubes and tips are connected to six peripheral fins (see Fig. 2). The finned surface is composed of three levels of fin arrangement, each characterized by the length of radial fin and mounted with a 30° offset from its neighboring level. In a recent paper [7], we carried out an experimental evaluation of the PFT heat exchanger performance. Five prototypes with different values of radial fin length, fin thickness, heat exchanger flow length, face area, and fin distribution were tested in a wind-tunnel calorimeter for air superficial velocities between 0.84 and 4.11 m/s. The heat transfer and pressure drop data were predicted by a 1-D model based on the theory of porous media that accounted for the heat transfer by conduction in the fins. The model incorporated correlations for the interstitial Nusselt number and friction factor in the determination of the heat transfer rate and pressure drop.

The optimum geometric configuration of a given heat exchanger can be achieved in a number of ways, which depend on the type of objective function, optimization algorithm and constraints that are applied. Shah and Sekulić [3] and Webb and Kim [4] presented general overviews of performance evaluation criteria (PEC) for heat transfer surfaces and heat exchangers with and without phase change. Yilmaz et al. [8,9] reviewed the existing first- and second-law based PEC. While the former usually employ miscellaneous types of objective function that relate the heat transfer performance and the pressure drop penalty, the latter are formulated so as to achieve a minimum entropy generation (or a minimum exergy destruction).

Bejan [10,11] demonstrated the use of entropy generation minimization (EGM) for optimization of different devices and systems, including heat exchangers. Hesselgreaves [12,13] reviewed several

* Corresponding author. Tel.: +55 48 3234 5691; fax: +55 48 3234 5166.
E-mail address: jrb@polo.ufsc.br (J.R. Barbosa Jr.).

0017-9310/$ - see front matter © 2012 Elsevier Ltd. All rights reserved.
http://dx.doi.org/10.1016/j.ijheatmasstransfer.2012.08.021

Nomenclature

A	surface area (m^2)
A_c	cross-section area (m^2)
c_p	specific heat capacity (J/kg K)
D_p	equivalent particle diameter (m)
E	heat exchanger effectiveness (–)
f	friction factor (–)
$\bar{h}$	average convection coefficient (W/m^2 K)
k	thermal conductivity (W/m K)
L	length (m)
$\dot{m}$	mass flow rate (kg/s)
N_S	entropy generation number (–)
Nu	Nusselt number (–)
P	pressure (Pa)
Pr	Prandtl number (–)
q'	heat rate per unit length (W/m)
q''	heat flux (W/m^2)
$\dot{Q}$	heat transfer rate (W)
Re	Reynolds number (–)
St	Stanton number (–)
$\dot{S}$	entropy generation rate (W/K)
T	temperature (K)
x	distance (m)
U_D	Darcean (superficial) velocity (m/s)
V	volume (m^3)
Greek	
ΔT_{lm}	log-mean temperature difference (K)
ε	porosity (–)
η_o	overall surface efficiency (–)
ν	kinematic viscosity (m^2/s)
ρ	density (kg/m^3)
Subscripts	
a	air
gen	generation
s	solid
w	wall

second-law based approaches of PEC and presented a rational calculation method by deriving new relations for the local rate generation process and for the nearly-balanced counterflow arrangement. Zimparov and Vulchanov [14] and Zimparov [15,16] developed extended PEC equations for enhanced heat transfer surfaces based on the entropy production theorem so as to include the effect of fluid temperature variation in a tubular heat exchanger. San and Jan [17] proposed a second-law analysis of a wet crossflow heat exchanger that used the maximum exergy recovery factor as a design criterion. Several researchers also investigated the effect of the channel geometry (cross-section, surface enhancement or insert type) on the entropy production due to heat transfer across a finite temperature difference and fluid friction [18–22]. Morosuk [20] investigated the entropy production in isothermal developing and developed laminar flows in pipes totally and partially filled with a porous medium. Mahmud and Fraser [21] quantified numerically the entropy production in a parallel-plate channel filled with a porous medium. Khan and Yovanovich [23] applied the EGM method to study the thermodynamic losses caused by heat transfer and pressure drop in the air flow in a cylindrical pin-fin heat sink considering the effect of flow by-pass. Tasnim et al. [24] evaluated the entropy generation in the porous regenerator of a thermoacoustic refrigerator, and concluded that the highest heat removal rates in the refrigerator corresponded to the minimum entropy generation rates in the regenerator. Hermes et al. [25] developed an EGM-based method to optimize air-cooled finned-tube condensers for light-commercial refrigeration applications.

The purpose of this paper is to combine the experimentally validated modeling framework of Pussoli et al. [7] for the air-side heat transfer and pressure drop with the entropy generation minimization (EGM) theory of Bejan [10] to determine the optimum characteristics of PFT heat exchangers. The fixed geometry, fixed face area and variable geometry performance evaluation criteria (PEC) of Webb and Kim [4] were applied for boundary conditions of prescribed wall temperature and wall heat flux. In all situations, it was possible to determine a combination of independent parameters that provided a minimum entropy generation rate.

2. Modeling

For high absolute temperature flows, the entropy generation rate per unit length in a heat exchanger can be computed through the following equation [10]:

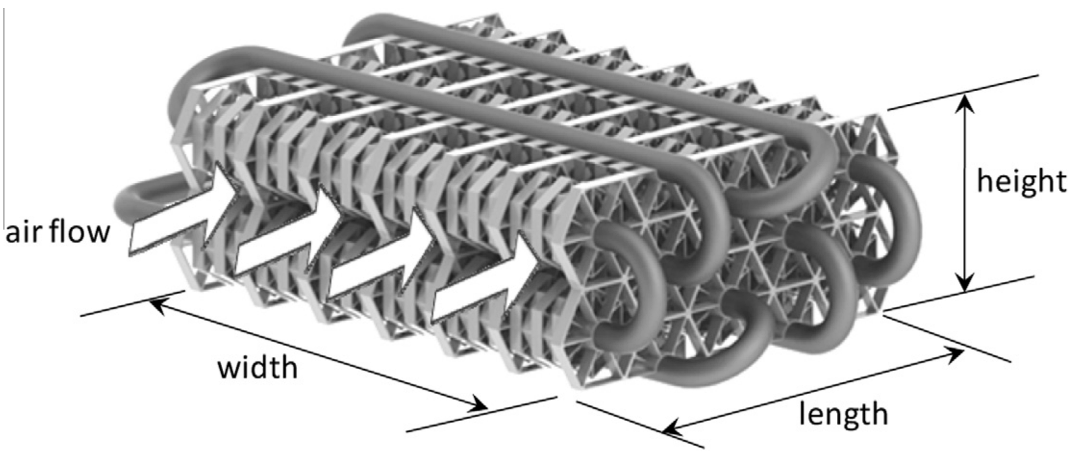

Fig. 1. The peripheral finned-tube geometry [7].

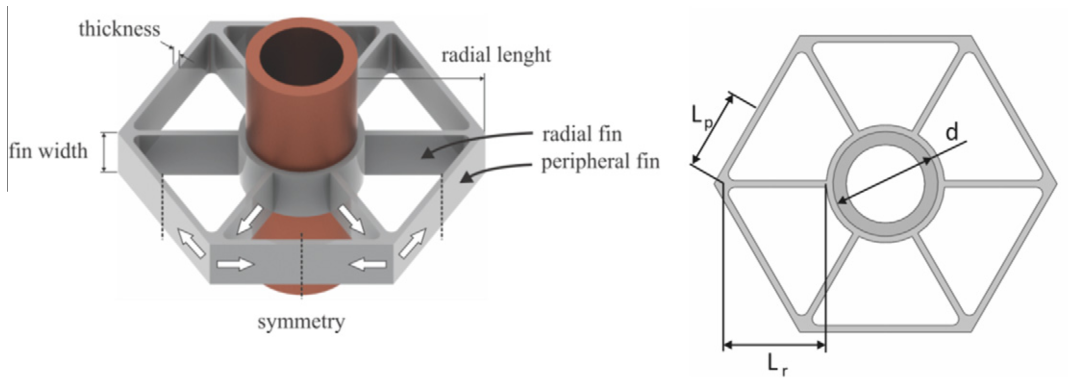

Fig. 2. Fin geometric parameters [7].

Table 1
Parameters and constraints of the optimization analysis.

PEC	Heat transfer rate (W)	Overall surface efficiency (–)	Face area (m^2)	Heat exchanger length (m)	Particle diameter (m)	Porosity (–)	Air mass flow rate (kg/s)	Air-side surface area (m^2)
FG-CT-1	300	0.8	0.008	0.1123	Variable	0.85	Output	Output
FG-CT-2	300	0.8	0.008	0.1123	0.0015	Variable	Output	Output
FG-CH	300	0.8	0.008	0.1123	Variable	0.85	Output	Output
FA-CT	300	0.8	0.008	Output	0.002	0.85	0.01	Output
FA-CH	300	0.8	0.008	Output	0.002	0.85	0.01	Output
VG-CT	300	0.8	Output	Output	0.002	0.85	0.01	0.8086
VG-CH	300	0.8	Output	Output	0.002	0.85	0.01	0.8086

$$\dot{S}'_{gen} = \dot{S}'_{gen,\Delta T} + \dot{S}'_{gen,\Delta P} = \frac{q'(T_w - T_a)}{T_a^2} + \frac{\dot{m}_a}{\rho_a T_a}\left(-\frac{dP}{dx}\right) \tag{1}$$

where the first term is associated with the generation of entropy due to heat transfer across a finite temperature difference and the second is due to fluid friction. In the PFT geometry, due to the large number of geometric variables involved (three levels of radial fin length, thickness and width) the optimization was carried out in terms of three parameters, namely, porosity, particle Reynolds number and equivalent particle diameter. The two fundamental boundary conditions of constant wall temperature and wall heat flux were evaluated.

2.1. Constant wall temperature

This limiting case approximates to that of an evaporator with a negligible combined thermal resistance of internal convection and wall conduction. The first term on the right of Eq. (1) can be replaced by

$$\dot{S}'_{gen,\Delta T} = \eta_0 \bar{h} \frac{(T_w - T_a)^2}{T_a^2}\frac{dA}{dx} \tag{2}$$

where the air-side heat transfer coefficient is given by

$$\bar{h} = \frac{\dot{m}_a c_{pa} \mathrm{St}}{A_c \varepsilon} = \frac{\dot{m}_a c_{pa}}{A_c \varepsilon}\frac{\mathrm{Nu}_{D_p}}{\mathrm{Re}_{D_p}\mathrm{Pr}} \tag{3}$$

and the rate of change of the surface area with distance can be calculated as

$$\frac{1}{A_c}\frac{dA}{dx} = \frac{dA}{dV_s}\frac{dV_s}{dV} = \frac{6}{D_p}(1-\varepsilon) \tag{4}$$

The pressure gradient in the porous medium can be calculated as follows [26]:

$$-\frac{dP}{dx} = f\frac{\rho U_D^2}{D_p}\frac{(1-\varepsilon)}{\varepsilon^3} \tag{5}$$

Therefore, in dimensionless form, Eq. (1) can be written in terms of the entropy generation number as follows:

$$\frac{dN_s}{dx} = \frac{d}{dx}\left(\frac{\dot{S}_{gen}}{\dot{m}_a c_{pa}}\right) = \eta_0 \frac{6\mathrm{St}}{D_p}\frac{(1-\varepsilon)}{\varepsilon}\frac{(T_w - T_a)^2}{T_a^2} + f\frac{\mathrm{Re}_{D_p}^2 \nu_a^2}{D_p^2 c_{p,a} T_a}\frac{(1-\varepsilon)^3}{\varepsilon^3} \tag{6}$$

Assuming that the overall surface efficiency and the physical properties remain constant (they were estimated at the log-mean temperature between the inlet and outlet), the air-side entropy generation number for the heat exchanger (the objective function) is given by

$$N_s = \eta_0 \frac{6\mathrm{St}}{D_p}\frac{(1-\varepsilon)}{\varepsilon}\int_0^L \frac{(T_w - T_a)^2}{T_a^2}dx + f\frac{\mathrm{Re}_{D_p}^2 \nu_a^2}{D_p^3 c_{p,a}}\frac{(1-\varepsilon)^3}{\varepsilon^3}\int_0^L \frac{1}{T_a}dx \tag{7}$$

where the air temperature distribution is given by

$$\frac{T_w - T_a}{T_w - T_{a,in}} = \exp\left[-\left(\frac{\eta_0 \bar{h} A}{\dot{m}_a c_{pa}}\right)\frac{x}{L}\right] \tag{8}$$

2.2. Constant heat flux

This case approximates to that of a balanced heat exchanger, i.e., one in which the thermal capacity rates of both streams are identical. The rate of entropy generation due to heat transfer is written in the form [10]:

$$\dot{S}'_{gen,\Delta T} = \frac{q''^2}{\eta_0 \bar{h} T_a^2}\frac{dA}{dx} \tag{9}$$

where the heat flux is computed as the ratio of the heat transfer rate (a fixed constraint in the analysis) and the air-side surface area. After an algebraic manipulation of Eqs. (1) and (9), with the friction term identical to that in Eq. (6), the following relationship can be obtained for the rate of change of the entropy generation number

$$\frac{dN_s}{dx} = \frac{6q''^2 D_p \varepsilon}{\eta_0 \mathrm{Pr}^2 k_a^2 T_a^2 \mathrm{St}(1-\varepsilon)\mathrm{Re}_{D_p}^2} + f\frac{\mathrm{Re}_{D_p}^2 \nu_a^2}{D_p^3 c_{p,a} T_a}\frac{(1-\varepsilon)^3}{\varepsilon^3} \quad (10)$$

Again, assuming constant physical properties and overall surface efficiency, one has

$$N_s = \frac{6q''^2 D_p \varepsilon}{\eta_0 \mathrm{Pr}^2 k_a^2 \mathrm{St}(1-\varepsilon)\mathrm{Re}_{D_p}^2}\int_0^L \frac{1}{T_a^2}dx + f\frac{\mathrm{Re}_{D_p}^2 \nu_a^2}{D_p^3 c_{p,a}}\frac{(1-\varepsilon)^3}{\varepsilon^3}\int_0^L \frac{1}{T_a}dx \quad (11)$$

where the temperature distribution in the constant heat flux case is given by

$$T_a = T_{a,in} + \frac{6q''}{\mathrm{Pr} k_a \mathrm{Re}_{D_p}} x \quad (12)$$

It is worth mentioning that the same friction factor and Nusselt number relationships were used in the constant wall temperature and constant wall heat flux cases.

2.3. Computational implementation and closure relationships

A computer program was written on the EES platform [27] in order to perform the numerical integration of Eqs. (7) and (11). Due to their predictions of the PFT heat exchanger experimental data with RMS errors smaller than 1% (heat transfer) and 3% (pressure drop) [7], the correlations of Handley and Heggs [28] and Montillet et al. [29] for the Nusselt number and friction factor were chosen. These are given by

$$\mathrm{Nu}_{D_p} = \frac{0.255}{\varepsilon}\mathrm{Pr}^{1/3}\mathrm{Re}_{D_p}^{2/3} \quad (13)$$

$$f = a\left(\frac{D}{D_p}\right)^{0.2}\left\{\frac{1000}{\mathrm{Re}_{D_p}(1-\varepsilon)} + \frac{60}{[\mathrm{Re}_{D_p}(1-\varepsilon)]^{0.5}} + 12\right\} \quad (14)$$

where a is equal to 0.050 since the porosity, ε, is larger than 0.4 [29]. D is the equivalent diameter of the air-side passage. In addition to the porosity, the particle-based Reynolds number and the equivalent particle diameter were chosen as independent variables in the optimization exercise. These are defined as

$$\mathrm{Re}_{D_p} = \frac{U_D D_p}{\nu_a(1-\varepsilon)} \quad (15)$$

$$D_p = \frac{6V_s}{A} \quad (16)$$

The equivalent particle diameter is the (micro) characteristic length scale of porous media in single-phase flow [30]. For this reason, it was decided that it should be left as a dimensional parameter in the present analysis, since it would be somewhat artificial to define another (constant) length scale just for the sake of using it to non-dimensionalize the equivalent particle diameter.

3. Results

Results were generated for the three PEC proposed by Webb and Kim [4]: *fixed geometry*, **FG** (when the face area and the heat exchanger length are kept fixed during the optimization), *fixed face area*, **FA** (when the face area is held constant, but the heat exchanger length is free to vary), and *variable geometry*, **VG** (when both the face area and the heat exchanger length are free to vary). Table 1 summarizes the cases evaluated in the present study, where the values of the parameters are similar to those investigated experimentally [7]. **CT** and **CH** stand for constant wall temperature and constant heat flux, respectively. The air inlet temperature needed to compute the physical properties is assumed equal to 0 °C for all cases. The overall surface efficiency was assumed constant since no knowledge of the actual fin structure or dimensions is needed in order to perform the optimization analysis. Moreover, as η_o is only moderately affected by the operating conditions [7], this assumption seems plausible given the other simplifications already made in this conceptual evaluation of the PFT heat exchanger.

3.1. Fixed geometry

The results for the **FG-CT-1** case are shown in Fig. 3. For each D_p value between 1 and 5 mm, there is a particular Re_{D_p} that yields a minimum total entropy generation rate, which is the sum of individual rates due to heat transfer and pressure drop. The value of this minimum rate Re_{D_p} increases with the particle diameter. Here, an increase in D_p is only possible if the air-side surface area decreases. In practice, this can be achieved by reducing the length and increasing the thickness of the smaller fin arrangements in such a way that the solid volume remains constant. For a given value of Re_{D_p}, increasing the particle diameter means that the superficial air velocity must decrease and, for a fixed face area, the resulting decrease in mass flow rate causes an increase in the outlet air temperature. Since the heat transfer rate is a constraint, the upshot is that the internal fluid temperature must increase accordingly, which contributes to raising the rate of entropy generation due to heat transfer across a finite temperature difference.

Fig. 4 shows the results for case **FG-CT-2**. With the overall dimensions and D_p kept fixed, an increase in porosity is such that the associated reduction in the solid volume must be accompanied by a decrease in the surface area, since D_p must be kept constant. Analogous to the **FG-CT-1** case, for a given Re_{D_p}, an increase in porosity leads to a reduction of the superficial velocity (and mass flow rate). Thus, if Re_{D_p} is less than the one linked to the minimum N_S, an increase in the rate of entropy generation due to finite temperature difference heat transfer is observed because the internal fluid temperature must increase so as to meet the fixed heat transfer rate constraint.

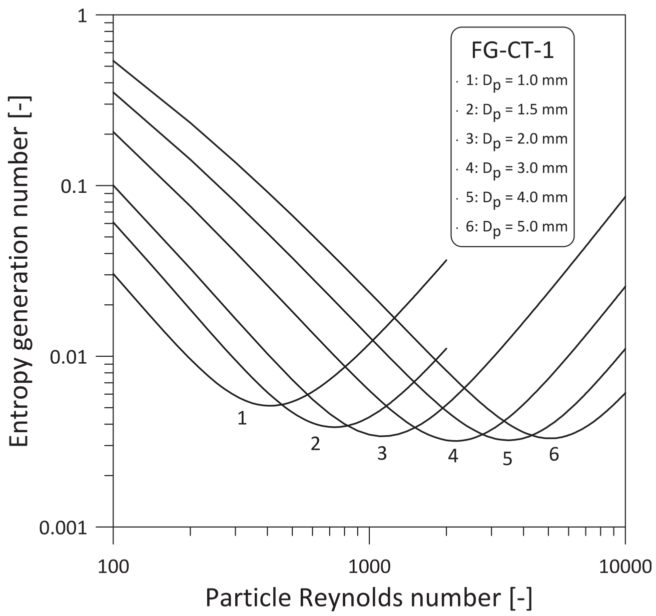

Fig. 3. N_S results for the **FG-CT-1** case.

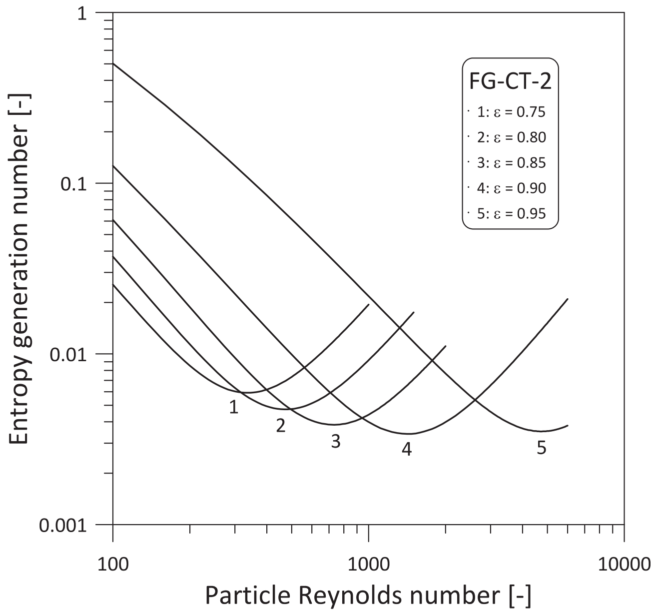

Fig. 4. N_S results for the **FG-CT-2** case.

Fig. 5 shows the behavior of the minima N_S (shown in Fig. 3) as a continuous function of the particle diameter, and points out the existence of a global minimum N_S for the **FG-CT-1** case. A global minimum, in this case, means that a specific value of D_p is uniquely associated with the smallest value of N_S for a given set of constraints. A similar plot can be produced for the **FG-CT-2** case by having the porosity in the abscissas. As can be seen, the slope of the curve is less pronounced for values of D_p larger than that associated with the global minimum N_S (approximately 3 mm). This finding can be combined with the result for the air-side pumping power (Fig. 6), which also has a global minimum, to determine the best range of operating conditions and/or geometry of the PFT heat exchanger.

The results for the **FG-CH** case are shown in Figs. 7 and 8. As the particle diameter increases, the surface area must decrease to maintain the porosity constraint. Because the heat transfer rate is also constrained, the heat flux must increase accordingly. Besides, the increase in D_p is also followed by a reduction in superficial velocity for a given Re_{D_p}. Therefore, as in the **FG-CT** cases, Fig. 7 shows that increasing D_p causes an increase in the rate of entropy generation due to heat transfer, which may contribute to increasing the total entropy generation rate if the particle Reynolds number is lower than that associated with the minimum N_S. Fig. 8 shows that a global minimum also exists for the **FG-CH** case, although it is much less sharper than in the constant temperature cases.

3.2. Fixed face area

In the **FA-CT** and **FA-CH** cases, the mass flow rate is kept fixed and the optimum heat exchanger length can be defined based on the trade-off in entropy generation rate due to heat transfer across a finite temperature difference between the streams and air-side pressure drop. A typical application of the **FA-CT** PEC is the component-level optimization of evaporators for domestic and light commercial refrigerators and freezers, where the cooling capacity may be seen as a design constraint and the face area is fixed due to cabinet space restrictions and positioning of the fan relative to the evaporator.

Figs. 9 and 10 show the results obtained for the **FA-CT** case. In Fig. 9, the heat exchanger length is given in terms of the number of transfer units defined as

$$NTU = \frac{\eta_0 \bar{h} A}{\dot{m}_a c_{pa}} = \frac{\dot{Q}}{\Delta T_{lm}} \frac{1}{\dot{m}_a c_{pa}} \tag{17}$$

where ΔT_{lm} is the log-mean temperature difference which, for the **CT** cases, is given by

$$\Delta T_{lm} = \frac{T_{a,in} - T_{a,out}}{ln\left(\frac{T_{a,in} - T_w}{T_{a,out} - T_w}\right)} \tag{18}$$

The minimum entropy generation number takes place at $NTU = 1.55$, which corresponds to a heat exchanger effectiveness of 0.78. The effectiveness is defined as the ratio of the heat transfer rate to the maximum heat transfer rate as follows:

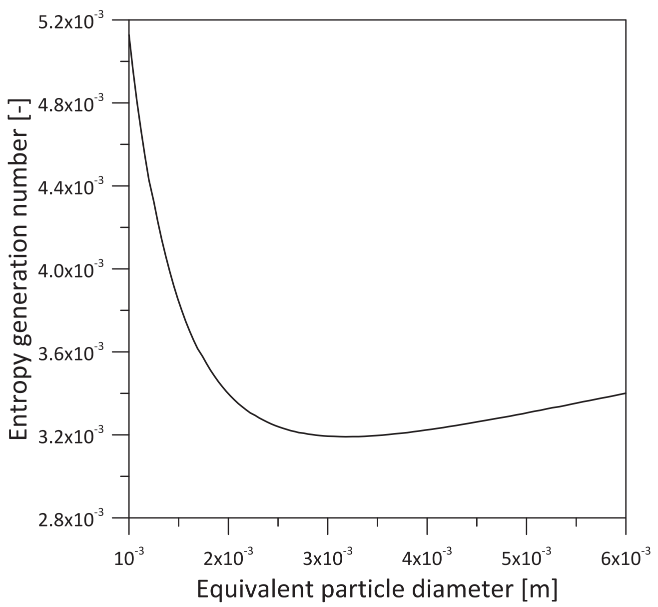

Fig. 5. Global minimum for the **FG-CT-1** case.

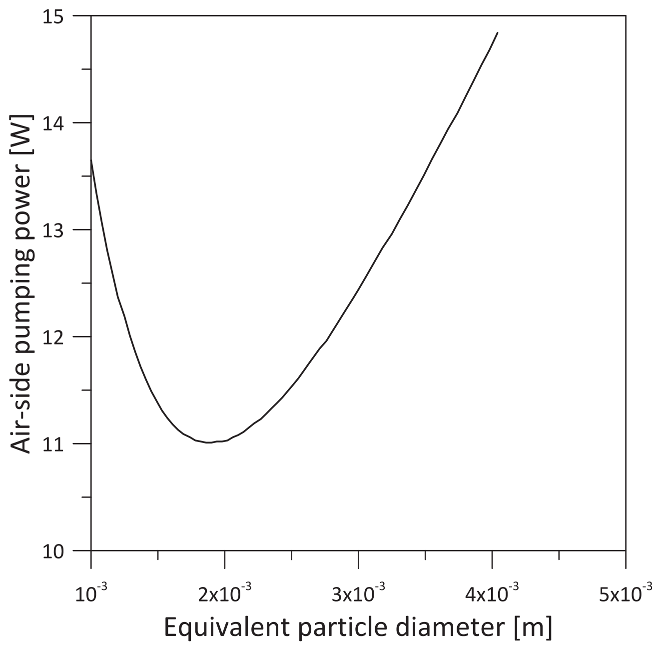

Fig. 6. Air-side pumping power behavior for the **FG-CT-1** case.

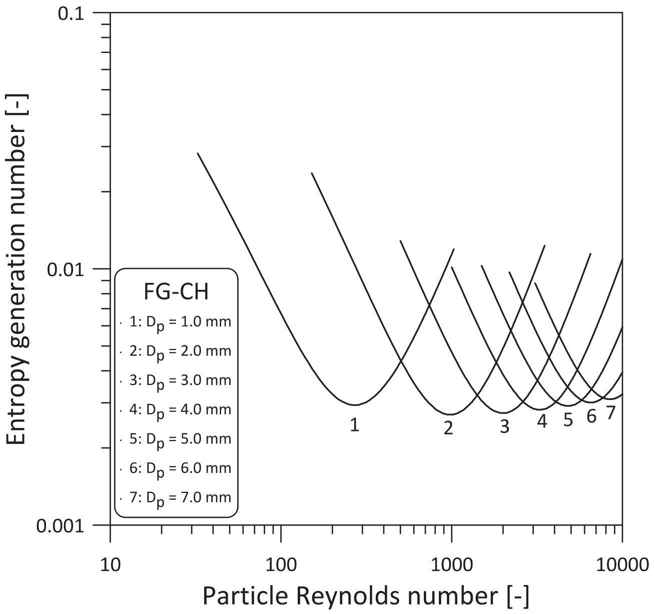

Fig. 7. N_S results for the **FG-CH** case.

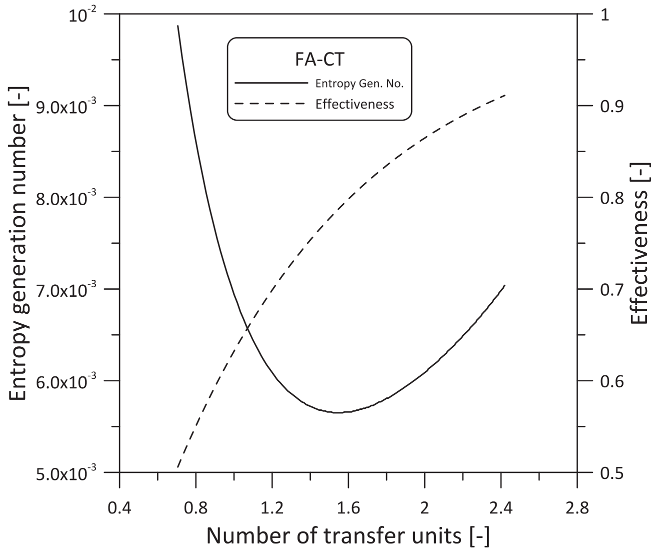

Fig. 9. N_S results for the **FA-CT** case.

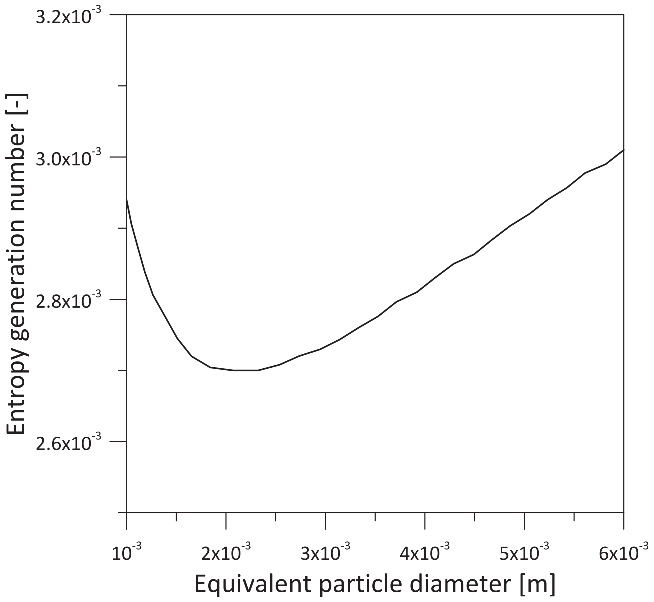

Fig. 8. Global minimum for the **FG-CH** case.

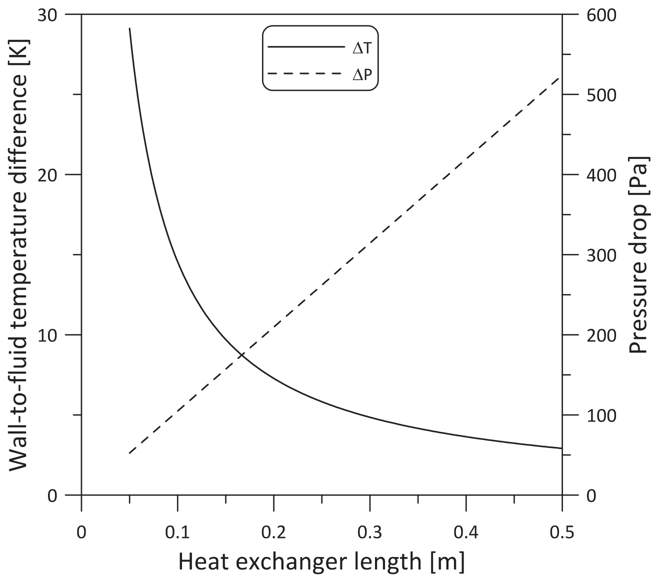

Fig. 10. Temperature difference and pressure drop results for the **FA-CT** case.

$$E = \frac{\dot{Q}}{\dot{m}_a c_{pa}(T_{a,in} - T_w)} \tag{19}$$

It can be inferred from Fig. 9 that, since the effectiveness increases monotonically with the *NTU*, it does not necessarily provide the best thermal-hydraulic configuration, nor is it a suitable performance evaluation parameter, because it does not take the fluid pumping power into account [31].

In the **FA-CT** case, the minimum N_S takes place when the heat exchanger length is 0.181 m. Since the mass flow rate is also kept fixed, both Re_{D_p} and the superficial air velocity remain constant. As the heat exchanger length increases, the air temperature decreases because of the associated increase in surface area, which as a whole contributes to decreasing the finite temperature heat transfer contribution to the entropy generation rate (see Fig. 10). Nevertheless, a minimum N_S exists because of the pressure drop contribution, which increases linearly with the heat exchanger length. It should be noted that the wall-to-fluid temperature difference plotted for the **CT** cases (i.e., **FA** and **VG**) corresponds to the temperature difference at the heat exchanger outlet ($T_{a,out} - T_w$).

In the **FA-CH** case (Figs. 11 and 12), a general behavior similar to that of the **FA-CT** situation is observed, but the minimum N_S occurs at a heat exchanger length of 0.266 m, and hence at a higher *NTU* of 5.4. For a constant heat flux (balanced heat exchanger), the log-mean temperature difference is equal to the local temperature difference between the fluid and the wall, which is a constant for a given heat exchanger length. In the **FA-CH** case, a constant heat transfer rate is guaranteed by a decrease in the local heat flux as the heat exchanger length increases. In this way, the temperature difference between the air and the wall decreases as a function of the heat exchanger length (Fig. 12).

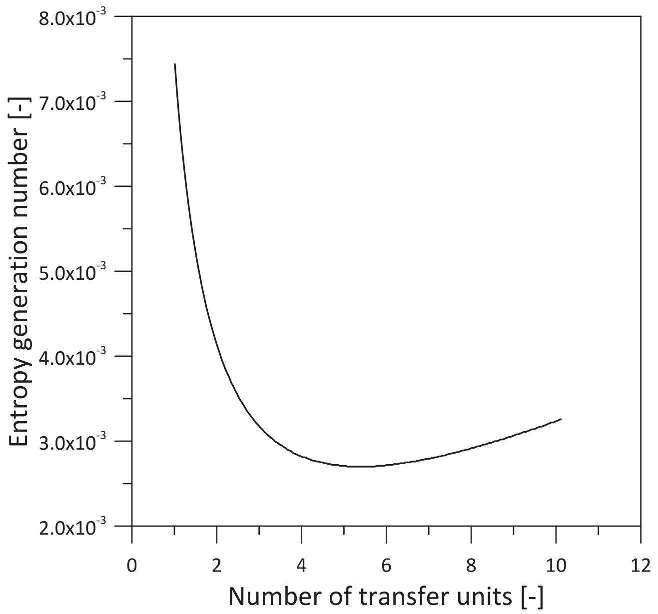

Fig. 11. N_S results for the **FA-CH** case.

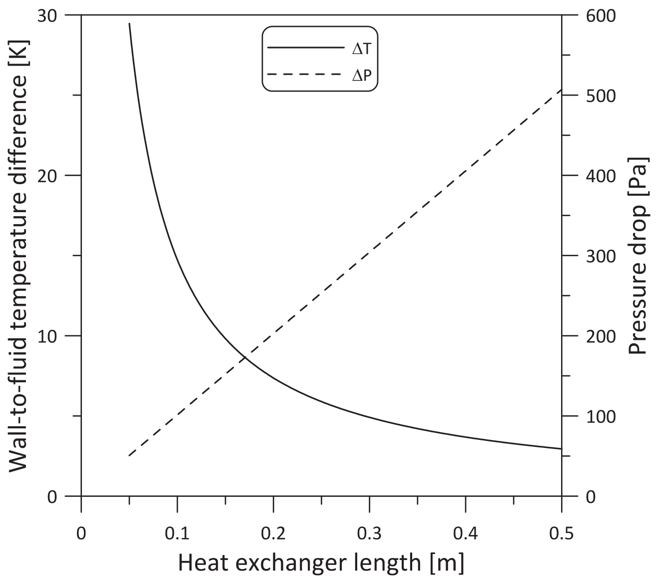

Fig. 12. Temperature difference and pressure drop results for the **FA-CH** case.

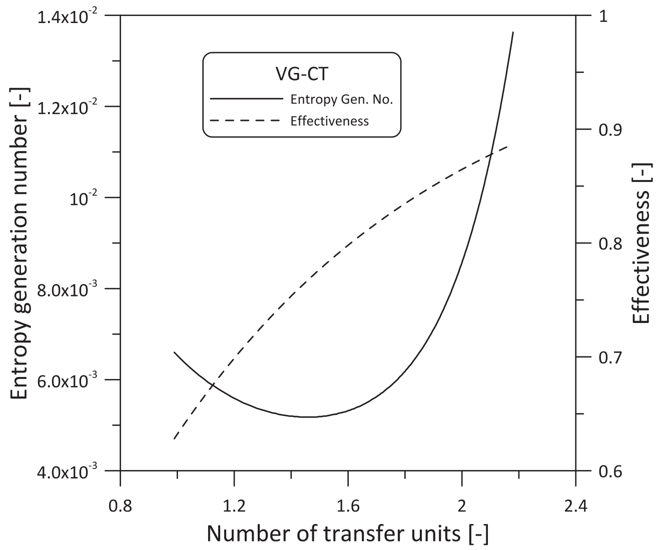

Fig. 13. N_S results for the **VG-CT** case.

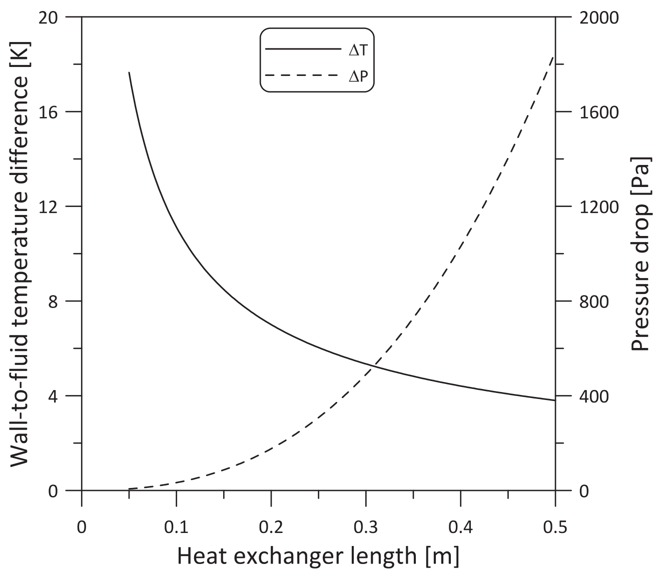

Fig. 14. Temperature difference and pressure drop results for the **VG-CT** case.

3.3. Variable geometry

This criterion is applicable when changes in the overall dimensions of the heat exchanger are allowed. In the present analysis, it was necessary to constrain, in addition to the heat transfer rate, the total surface area of the heat exchanger (tubes and fins), as can be seen in Table 1. This guarantees that the heat exchanger length and the face area are interdependent and, by changing these variables over an appropriate range, the minimum entropy generation rate can be determined.

In the **VG-CT** case shown in Figs. 13 and 14, the minimum N_S is achieved with a heat exchanger length of 0.137 m and a face area of 0.0132 m^2. The behavior of the entropy generation number and of the heat exchanger effectiveness (Eq. (19)) as a function of the *NTU* is also shown. The minimum entropy generation number occurs at *NTU* = 1.46, which corresponds to a heat exchanger effectiveness of 0.76.

In the **VG-CT** case, as the heat exchanger length is increased, the face area must be reduced in order to satisfy the surface area, porosity and equivalent particle diameter constraints. This reduction in face area is accompanied by an increase in the air superficial velocity and Re_{D_p} (and local heat transfer coefficient) because the mass flow rate is also a constraint. This contributes to decreasing the temperature difference between the streams and, consequently, the rate of entropy generation due to heat transfer. However, again, as the heat exchanger length increases and the face area decreases, the associated increase in air superficial velocity and pressure gradient contributes to increasing the pressure drop and its contribution to the entropy generation rate.

For the **VG-CH** case shown in Figs. 15 and 16, the minimum entropy generation number occurs for a heat exchanger length of 0.1654 m and a face area of 0.0102 m^2. The corresponding number of transfer units is 3.70. As in the **VG-CT** case, the increase in the heat exchanger length reduces the face area and augments the

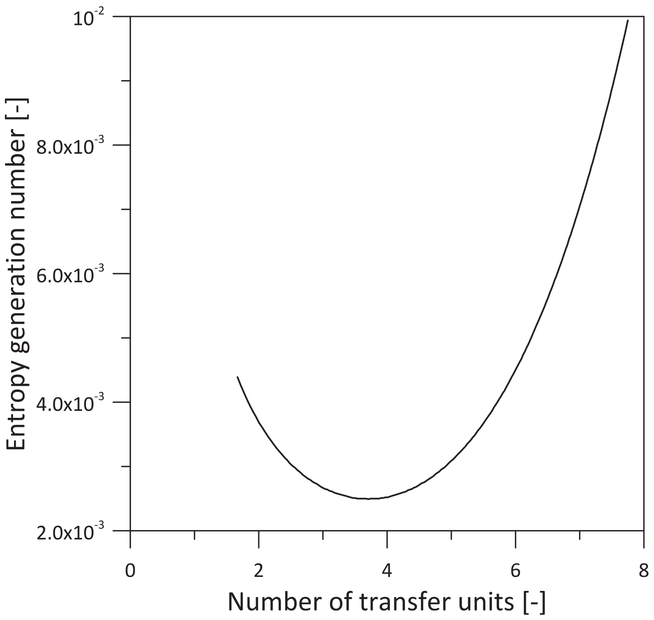

Fig. 15. N_S results for the **VG-CH** case.

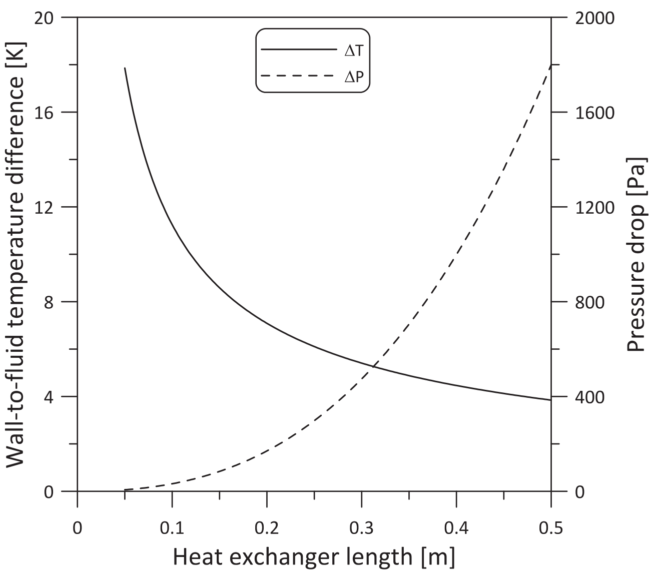

Fig. 16. Temperature difference and pressure drop results for the **VG-CH** case.

air velocity. The main feature of the **VG-CH** case is that, irrespectively of the length-face area combination, the local heat flux will always remain unchanged. In no other situation evaluated in the present work, the heat flux was independent of the other constraints.

4. Conclusions

An extensive EGM-based optimization analysis of the peripheral finned-tube extended surface geometry has been conducted in this paper. The analysis made use of the fixed geometry (**FG**), fixed face area (**FA**) and variable geometry (**VG**) PEC of Webb and Kim [4] for both the constant wall temperature and constant heat flux boundary conditions. Due to the large number of geometric variables involved in the peripheral finned-tube heat exchanger, the analysis was focused on the three main parameters associated with the fluid flow and heat transfer in the porous medium, i.e., porosity, equivalent particle diameter and particle-based Reynolds number. Closure relationships for the interstitial Nusselt number and friction factor needed in the analysis were those due to Handley and Heggs [28] and Montillet et al. [29] because of their satisfactory performance in correlating the heat transfer and pressure drop experimental data in real peripheral finned-tube heat exchanger prototypes [7].

It is worth emphasizing that the performance measures and the analysis in general are applicable not only to peripheral finned-tube heat exchangers, but to any heat exchanger where the air-side thermal-hydraulic characteristics can be modeled with Eqs. (13) and (14) for the interstitial Nusselt number and friction factor.

For a fixed heat transfer rate (cooling capacity) of 300 W, which is typical of light commercial refrigeration applications, and other constraints that depended on the PEC under analysis (**FG**, **FA** or **VG**), it was possible to achieve a combination of independent parameters that provided a minimum entropy generation rate for all cases evaluated.

It is also important to point out that the "entropy generation paradox" [10,11,13] associated with the definition of the entropy generation number used in the present paper [10] will only exist when the heat transfer rate (heat duty) is unfixed and when the entropy generation rate due to fluid friction is negligible in comparison with the term due to heat transfer across a finite temperature difference. This is not the case here, since the heat duty was a fixed constraint and the pressure drop contribution to entropy generation was non-negligible. Furthermore, it was shown in this paper that (i) there is an optimum *NTU* associated with a minimum entropy generation number for both types of heat transfer boundary condition and (ii) the heat exchanger effectiveness is not a suitable performance parameter to evaluate the heat exchanger performance because it increases monotonically with the *NTU* and does not take into account the fluid pumping power through the heat exchanger. This is in line with recent independent findings [31].

Acknowledgements

The material presented in this paper is a result of a long-standing technical-scientific partnership between UFSC and Embraco. Financial support from FINEP and CNPq through Grant No. 573581/2008-8 (National Institute of Science and Technology in Cooling and Thermophysics) is duly acknowledged.

References

[1] C.-C. Wang, Technology review – a survey of recent patents of fin-and-tube heat exchangers, J. Enhanc. Heat Transfer 7 (2000) 333–345.
[2] C.-C. Wang, A survey of recent patents on fin-and-tube heat exchangers from 2001 to 2009, Int. J. Air Cond. Refrig. 18 (2010) 1–13.
[3] R.K. Shah, D. Sekulić, Fundamentals of Heat Exchanger Design, Wiley, New York, 2003.
[4] R.L. Webb, N.-H. Kim, Principles of Enhanced Heat Transfer, second ed., Taylor and Francis, New York, 2005.
[5] J.R. Thome, Heat Transfer to Air-Cooled Heat Exchangers, Wolverine Heat Transfer Engineering Data Book III, 2010 (Chapter 6). Available from: <http://www.wlv.com/products/thermal-management-databooks.html>.
[6] H. Wu, D. Ma, M. Kaviany, Peripheral fins for blockage robustness, Int. J. Heat Mass Transfer 50 (2007) 2514–2520.
[7] B.F. Pussoli, J.R. Barbosa Jr., L.W. da Silva, M. Kaviany, Heat transfer and pressure drop characteristics of peripheral-finned tube heat exchangers, Int. J. Heat Mass Transfer 55 (2012) 2835–2843.
[8] M. Yilmaz, O. Comakli, S. Yapici, O.N. Sara, Performance evaluation criteria for heat exchangers based on first law analysis, J. Enhanc. Heat Transfer 12 (2005) 121–157.
[9] M. Yilmaz, S. Karsli, O.N. Sara, Performance evaluation criteria for heat exchangers based on second law analysis, Int. J. Exergy 1 (2001) 278–294.
[10] A. Bejan, Entropy Generation through Heat and Fluid Flow, Wiley, New York, 1982.
[11] A. Bejan, Entropy generation minimization: the new thermodynamics of finite-size devices and finite-time processes, Appl. Phys. Lett. 79 (1996) 1191–1218.

[12] J.E. Hesselgreaves, Rationalization of second law analysis of heat exchangers, Int. J. Heat Mass Transfer 43 (2000) 4189–4204.
[13] J.E. Hesselgreaves, Compact Heat Exchangers: Selection, Design and Operation, Pergamon, 2001.
[14] V.D. Zimparov, N.L. Vulchanov, Performance evaluation criteria for enhanced heat transfer surfaces, Int. J. Heat Mass Transfer 37 (1994) 1807–1816.
[15] V.D. Zimparov, Extended performance evaluation criteria for enhanced heat transfer surfaces: heat transfer through ducts with constant wall temperature, Int. J. Heat Mass Transfer 43 (2000) 3137–3155.
[16] V.D. Zimparov, Extended performance evaluation criteria for enhanced heat transfer surfaces: heat transfer through ducts with constant heat flux, Int. J. Heat Mass Transfer 44 (2001) 169–180.
[17] J.Y. San, C.L. Jan, Second-law analysis of a wet crossflow heat exchanger, Energy 25 (2000) 939–955.
[18] Y. Demirel, R. Kahraman, Entropy generation in a rectangular packed duct with wall heat flux, Int. J. Heat Mass Transfer 42 (1999) 2337–2344.
[19] I. Dağtekin, H.F. Öztop, A.Z. Şahin, An analysis of entropy generation through a circular duct with different shaped longitudinal fins for laminar flow, Int. J. Heat Mass Transfer 48 (2005) 171–181.
[20] T.V. Morosuk, Entropy generation in conduits filled with porous medium totally and partially, Int. J. Heat Mass Transfer 48 (2005) 2548–2560.
[21] S. Mahmud, R.A. Fraser, Flow, thermal, and entropy generation characteristics inside a porous channel with viscous dissipation, Int. J. Therm. Sci. 44 (2005) 21–32.
[22] T.A. Jankowski, Minimizing entropy generation in internal flows by adjusting the shape of the cross-section, Int. J. Heat Mass Transfer 52 (2009) 3439–3445.
[23] W.A. Khan, M.M. Yovanovich, Optimization of pin-fin heat sinks in bypass flow using entropy generation minimization method, in: Proc. IPACK2007, ASME InterPACK '07, Vancouver, BC, Canada, Paper IPACK2007-33983, 2007.
[24] S.H. Tasnim, S. Mahmud, R.A. Fraser, Second law analysis of porous thermoacoustic stack systems, Appl. Therm. Eng. 31 (2011) 2301–2311.
[25] C.J.L. Hermes, W.L. Silva Jr., F.A.G. Castro, Thermal-hydraulic design of fan-supplied tube-fin condensers for refrigeration cassettes aimed at minimum entropy generation, Appl. Therm. Eng. 36 (2012) 307–313.
[26] M. Kaviany, Essentials of Heat Transfer, Cambridge University Press, New York, 2011.
[27] S.S. Klein, Engineering Equation Solver, Professional Version V8.528, 2010.
[28] D. Handley, P.J. Heggs, Momentum and heat transfer mechanisms in regular shaped packings, Trans. Inst. Chem. Eng. 46 (1968). paper T251.
[29] A. Montillet, E. Akkari, J. Comiti, About a correlating equation for predicting pressure drops through packed beds of spheres in a large range of Reynolds numbers, Chem. Eng. Process. 46 (2007) 329–333.
[30] M. Kaviany, Principles of Heat Transfer in Porous Media, Springer, 1995.
[31] C.J.L. Hermes, Conflation of ε-NTU and EGM design methods for heat exchangers with uniform wall temperature, Int. J. Heat Mass Transfer 55 (2012) 3812–3817.